COMPUTER SIMULATION OF FLAGELLAR MOVEMENT

VI. Simple Curvature-Controlled Models Are Incompletely Specified

CHARLES J. BROKAW
Division of Biology, California Institute of Technology, Pasadena, California 91125

ABSTRACT Computer simulation is used to examine a simple flagellar model that will initiate and propagate bending waves in the absence of viscous resistances. The model contains only an elastic bending resistance and an active sliding mechanism that generates reduced active shear moment with increasing sliding velocity. Oscillation results from a distributed control mechanism that reverses the direction of operation of the active sliding mechanism when the curvature reaches critical magnitudes in either direction. Bend propagation by curvature-controlled flagellar models therefore does not require interaction with the viscous resistance of an external fluid. An analytical examination of moment balance during bend propagation by this model yields a solution curve giving values of frequency and wavelength that satisfy the moment balance equation and give uniform bend propagation, suggesting that the model is underdetermined. At 0 viscosity, the boundary condition of 0 shear rate at the basal end of the flagellum during the development of new bends selects the particular solution that is obtained by computer simulations. Therefore, the details of the pattern of bend initiation at the basal end of a flagellum can be of major significance in determining the properties of propagated bending waves in the distal portion of a flagellum. At high values of external viscosity, the model oscillates at frequencies and wavelengths that give approximately integral numbers of waves on the flagellum. These operating points are selected because they facilitate the balance of bending moments at the ends of the model, where the external viscous moment approaches 0. These mode preferences can be overridden by forcing the model to operate at a predetermined frequency. The strong mode preferences shown by curvature-controlled flagellar models, in contrast to the weak or absent mode preferences shown by real flagella, therefore do not demonstrate the inapplicability of the moment-balance approach to real flagella. Instead, they indicate a need to specify additional properties of real flagella that are responsible for selecting particular operating points.

INTRODUCTION

The mechanism of oscillation in flagella and cilia is still unknown. In one suggested type of oscillatory mechanism, developed from ideas of Kinosita and Kamada (1939) and Machin (1958; 1963), the active sliding mechanism that generates bending is regulated by a result of active sliding, such as the curvature of the flagellum (Brokaw, 1971; 1972*a*). Oscillation will result if there is a delay in this feedback loop. A delay is inevitable in a sliding filament system because bending depends upon differences in sliding rate at different positions along the length, rather than sliding rate itself (Brokaw, 1971; 1972*a;* Shingyoji et al., 1977).

This oscillatory mechanism has been examined previously by computer simulation methods that solve the nonlinear, fourth-order, partial differential equation that is required to analyze the movement of an elastic filament in a viscous medium (Brokaw, 1972*b;* Hines and Blum, 1978; etc.). These methods have been used to show that flagellar models in which the active shear moment per unit length is regulated locally by flagellar curvature can initiate and propagate bending waves with features similar to real flagellar bending waves (Brokaw, 1972*b*). The response of these models to changes in the viscosity of the external medium shows a preference for particular modes of oscillation that is much stronger than is seen with real flagella (Brokaw, 1972*c;* etc.). The present paper attempts to explain this discrepancy. The analysis, like most previous flagellar modeling, is limited to bending in a plane, and does not attempt to explain the constraints that are responsible for generation of planar bending waves by flagella.

ANALYSIS

Moment Balance Analysis of Flagellar Bending

This analysis assumes that bending of a real flagellum represents the solution of a moment balance equation that balances active bending moments, $M_A(s, t)$ generated by an internal active sliding process against the elastic and viscous resistive moments, $M_E(s, t)$ and $M_V(s, t)$ resulting from the internal structural resistances of the flagellum and the external viscous resistances of the fluid in which it is moving. The moment balance equation for a flagellum

can be written

$$M_A(s, t) + M_E(s, t) + M_V(s, t) = 0. \quad (1)$$

In this equation, t represents time and s represents distance measured along the length of a flagellum, from the basal end. To use Eq. 1, the moments must be defined as functions of a variable such as the curvature, $\kappa(s, t)$, which completely describes the configuration of the flagellum as a function of time, and therefore completely describes its bending behavior. These functions include derivatives and integrals of $\kappa(s, t)$, such that Eq. 1 becomes a fourth-order partial differential equation.

Methods for numerical solution of this equation to obtain $\kappa(s, t)$ have been developed in previous work (Brokaw, 1972*b;* Hines and Blum, 1978). Most of the complexity of these procedures results from the integrations needed to obtain M_V.

Moment Balance with a Realistic Active Shear Process

One of the important characteristics of the best-known biological active shear system, skeletal muscle, is a force-velocity relationship that describes the decrease in force generated by the muscle as the shortening velocity increases. Some evidence indicates that the active shear system in flagella has similar characteristics (Brokaw, 1975*b*). The force-velocity behavior can be generated by detailed models for cross-bridges between the sliding microtubules of flagella, with explicit consideration of the kinetics of cross-bridge attachment and detachment, and these detailed models can be incorporated into flagellar models (e.g., Hines and Blum, 1979; Brokaw, 1982). To avoid the complications of such detailed models, I will introduce here a simpler prescription for the properties of an active shear system that is intended to mimic the properties of a cross-bridge system. Three assumptions are required. (*a*) In the absence of sliding, the active shear moment per unit length, m, has a constant value m_A. (*b*) In response to a very rapid change in shear, the moment-generating system behaves as a simple elastic shear resistance. This shear resistance mimics the stiffness of attached cross-bridges, which do not have time to detach and reattach during the rapid shear change. This shear resistance is determined by a parameter E_{SCB} that is independent of m_A. The actual shear resistance is the product of E_{SCB} and m_A, and E_{SCB} is therefore equal to the reciprocal of an amount of shear that will reduce the active shear moment to 0. $E_{SCB} = 4$ corresponds to reduction to 0 moment by a shear step of 0.25 rad, or an average of ~10 nm of sliding between tubules. (*c*) When $m \neq m_A$, for instance following a rapid shear change, there is a first-order recovery process by which m approaches m_A with a rate constant k_1. This system can be described by the following ordinary differential equation

$$dm/dt = -E_{SCB}|m_A|\dot{\sigma} + k_1(m_A - m), \quad (2)$$

where $\dot{\sigma} = d\sigma/dt$ is the shear rate. For constant shear rate, with $m_A > 0$, there is a steady-state solution

$$m = m_A(1 - E_{SCB}\dot{\sigma}/k_1). \quad (3)$$

This equation gives a linear decrease in m with increasing shear rate, and $m = 0$ when the shear rate $= k_1/E_{SCB}$.

For a time interval Δt in which the shear rate is constant, the solution to Eq. 2 can be written

$$m(t + \Delta t) = m(t) + [m_A - m(t)](1 - e^{-k_1\Delta t}) - |m_A|E_{SCB}\dot{\sigma}(1 - e^{-k_1\Delta t})/k_1. \quad (4)$$

Using the boundary condition of no sliding between flagellar doublet microtubules at the basal end of the flagellum, $\dot{\sigma}(0) = 0$, the shear rate, $\dot{\sigma}$, can be obtained from

$$\dot{\sigma}(s) = \int_0^s \dot{\kappa} ds, \quad (5)$$

where $\dot{\kappa} = d\kappa/dt$ is a local rate of bending.

Using the boundary condition of no restriction on sliding between flagellar doublet microtubules at the distal end of the flagellum ($s = S$) gives $M_A(S) = 0$, and $dM_A/ds = -m$ (Brokaw, 1971) allows $M_A(s, t + \Delta t)$ to be obtained from Eq. 4 by integration along the length. Because of Eq. 5, $M_A(s, t + \Delta t)$ will be a function of $\dot{\kappa}(s, t)$.

In the simplest situation, containing only a linear elastic bending resistance E_B, with a straight "rest position,"

$$M_E(s, t) = -E_B\kappa(s, t),$$

and

$$M_E(s, t + \Delta t) = -E_B\kappa(s, t) - E_B\dot{\kappa}\Delta t. \quad (6)$$

By inserting $M_E(s, t + \Delta t)$ and $M_A(s, t + \Delta t)$ into Eq. 1, a fully implicit solution can be obtained for the values of $\dot{\kappa}$ that will achieve moment balance at $t + \Delta t$. The numerical methods for obtaining this solution at intervals, Δs, along the length of the flagellar model are based on the methods of Brokaw (1972*b;* 1982). The term in Eq. 4 that contains $\dot{\sigma}$ is treated in the same manner as a viscous shear resistance.

A Simple Control Procedure Leads to Oscillation and Bend Propagation

In previous work using computer simulations to examine flagellar models, several procedures for control of the active shear moment system have been proposed that lead to oscillation and bend propagation. One of the simplest, based on models examined by Brokaw (1980; 1982), allows the constant m_A throughout each segment along the length of the flagellar model to have a value of either $+m_o$ or $-m_o$. The value of m_A is switched between these two values when the local curvature of the flagellum passes critical values. When the curvature falls below $-\kappa_o$, m_A becomes $+m_o$, and when the curvature rises above $+\kappa_o$, m_A becomes $-m_o$. In the jth segment $m_A(j)$ is controlled by the mean of

the values of $\kappa(j)$ and $\kappa(j-1)$ at the ends of the segment, using estimated values of κ at the midpoint of the next time step, obtained from $\kappa(t) + \frac{1}{2}[\kappa(t) - \kappa(t - \Delta t)]$.

Fig. 1 illustrates results obtained for a flagellar model containing this control procedure. Stable oscillation and bend propagation are obtained from this simple model containing only an elastic bending resistance and an active shear process, in the absence of external viscous resistance or any other internal resistances. However, this model has a serious defect, associated with the boundary condition that $\kappa = 0$ at $s = S$. In the joint closest to the distal end of the model, the curvature will never reach κ_0 if the active moment generated within the last segment is $< E_B\kappa_0$. This active moment will depend upon m_0 and Δs. If m_0 and Δs are too small relative to E_B and κ_0, the last segment will remain in the state in which it was started, and no oscillation will occur. This defect will gradually propagate towards the basal end of the flagellum, because if $\kappa(n-1)$ cannot reach $+\kappa_0$, so that $m_A(n)$ remains equal to $+m_0$, then $\kappa(n-2)$ will have difficulty in reaching $-\kappa_0$ when $m_A(n-1) = -m_0$, etc. To obtain the results shown in this paper, it was necessary to minimize this defect by modifying the control of active shear moment in the last segment and controlling $m_A(n)$ by $\kappa(n-1)$ rather than by the mean value of $\kappa(n-1)$ and $\kappa(n)$. The defect can be completely controlled by further modifications of this type. However, because of this defect, this particular form of curvature control, while useful for the purposes of this paper, is not a likely model for the control process in real flagella.

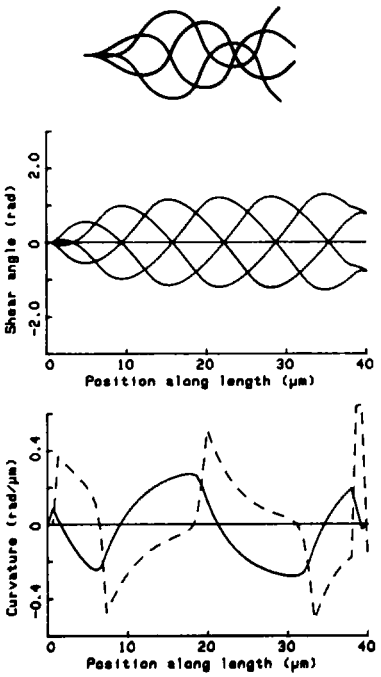

FIGURE 1 Behavior of a simple flagellar model. The parameters are $E_B = 2 \times 10^8$ pN nm^2, $m_0 = 20$ pN, $k_1 = 1{,}000$ s^{-1}, $E_{SCB} = 4$, and $\kappa_0 = 0.0002$ rad nm^{-1}. The flagellum is 40 μm in length, and oscillates with a frequency of 31 Hz. The *upper* panel shows the configuration of the model in the x, y, plane at time intervals separated by $\frac{1}{4}$ beat cycle. The basal end of the model has been arbitrarily maintained at fixed position and orientation. The *middle* panel shows shear curves giving the angular orientation of the flagellum as a function of length, at times corresponding to those in the upper panel. The lower panel shows curves for the curvature (solid line) and the active shear moment (dashed line) as functions of length, at one time in the beat cycle. The active shear moment curves are scaled so that the point on the ordinate representing a curvature of 0.4 rad μm^{-1} corresponds to a shear moment of 20 pN. Computations were performed on a microcomputer (9816; Hewlett-Packard Co., Palo Alto, CA), using HP-Pascal with 64-bit floating point arithmetic. The length of the flagellar model was divided into 60 segments, and 160 time steps were used per cycle of oscillation.

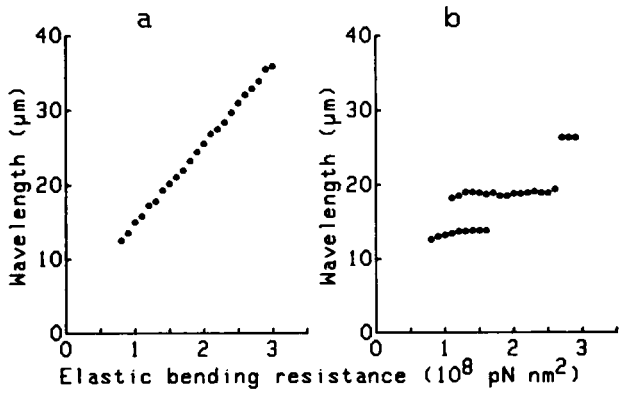

FIGURE 2 Effect of elastic bending resistance, E_B, on the wavelength of bending waves generated by the flagellar model shown in Fig. 1 (*a*) in the absence of external viscosity and (*b*) at a relative external viscosity of 8, with a small amount of elastic shear resistance added to the model (see text).

Changes in the value of the elastic bending resistance, E_B, cause a smooth variation in the wavelength of the motion. This change in wavelength is accompanied by an inverse change in the frequency of oscillation, but the propagation velocity V_S, equal to the product of frequency and wavelength, does not remain constant. Over the range illustrated in Fig. 2 *a*, V_S increased from 690 μm s^{-1} at $E_B = 1 \times 10^8$ pN nm^2 to 862 μm s^{-1} at $E_B = 3 \times 10^8$ pN nm^2. Computations with other variations of the model parameters indicate that the ratio, E_B/m_0, determines the wavelength, and that the frequency of oscillation is proportional to the maximum steady-state shear rate, k_1/E_{SCB}. The amplitude is primarily determined by the value of κ_0. Addition of a realistic value of linear elastic shear resistance, E_S, to the flagellar model has a relatively small effect on the steady-state solution shown in Fig. 1. With $E_S = 10$ pN at $E_B = 1 \times 10^8$ pN nm^2, the wavelength increases from 15.0 μm (Fig. 2 *a*) to 15.8 μm. The transient behavior of the flagellar model when started from a straight position by activating $m_A = +m_0$ throughout the length of the flagellum is more realistic when the flagellar model contains elastic shear resistance (not shown).

Analytical Examination of Oscillation

Since the flagellar model examined above does not contain any complicated external viscous terms, an analytical examination of some of its properties is possible. In a region

of the flagellum where m_A is constant and equal to $+m_o$, Eqs. 1 and 6 give

$$m = -E_B \, d\kappa/ds. \tag{7}$$

In the limiting case where k_1 and E_{SCB} are very large, Eqs. 3 and 7 give

$$-E_B \, d\kappa/ds = m_o (1 - E_{SCB} \dot{\sigma}/k_1). \tag{8}$$

If we assume that there is a solution for a propagated wave of curvature with constant properties, then, since $\kappa = d\sigma/ds$,

$$\dot{\sigma} = -V_S \kappa, \tag{9}$$

where V_S is the wave propagation velocity. This leads to a first-order differential equation for curvature

$$(E_B/m_o)d\kappa/ds + (V_S E_{SCB}/k_1)\kappa = -1. \tag{10}$$

E_B and m_o enter into the balance of bending moments only as the ratio E_B/m_o, and dimensional considerations then suggest that this ratio is likely to determine the wavelength of the solutions. The solution of Eq. 10 is a standard exponential relationship between κ and s. The region of constant m_A is one half-wave in length, in which κ goes from $+\kappa_o$ to $-\kappa_o$. This leads to

$$\ln[(1 + \kappa_o V_S E_{SCB} k_1)/(1 - \kappa_o V_S E_{SCB}/k_1)] = (m_o V_S E_{SCB} L)/(2 E_B k_1). \tag{11}$$

Since V_S equals the product of frequency, f, and wavelength, L, this solution yields a curve in the f, L plane, shown by the upper curve in Fig. 3.

This limiting case for large k_1 and large E_{SCB} cannot be compared directly with the flagellar computations using realistic values of k_1 and E_{SCB}. To use $E_{SCB} = 4$ and $k_1 = 1{,}000$, as in the model used to obtain the results shown in Figs. 1 and 2, it is necessary to go back to the two-point boundary value problem defined by Eqs. 2 and 7 and perform a numerical integration of both m and κ, starting with $\kappa = +\kappa_o$. When κ reaches $-\kappa_o$, the final value of m is compared with the initial value of m. Starting values of m are tried until a value is found such that the final value of m is equal to minus the starting value of m. This procedure is repeated for various values of V_S in order to construct the family of solutions corresponding to the lower solid curve in Fig. 3. This is a curve with the same general shape as the curve for the limiting case, but with lower values of f for a given L. Further computations with this procedure confirmed that the results approached the limiting case as higher values of E_{SCB} and k_1 were used.

Fig. 3 also shows a point corresponding to the values of f and L obtained from the computation for a flagellar model, shown in Fig. 1. This point lies close to the curve obtained with the same values of E_{SCB} and k_1 in Fig. 3.

The analysis leading to the curves in Fig. 3 suggests that there should be a family of solutions for each choice of the three parameters E_B/m_o, E_{SCB}/k_1, and κ_o. What factors are responsible for the selection of the particular solution obtained from the computation shown in Fig. 1? There is a major difference between the two approaches. Fig. 1 was obtained by solving an equation that balances bending moments; while the curves in Fig. 3 were obtained by balancing the first derivatives of the bending moments, so that some boundary conditions at the ends of the flagellum were ignored.

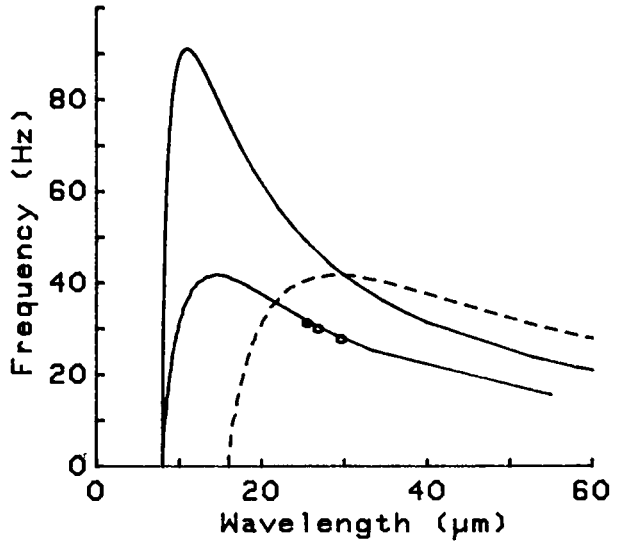

FIGURE 3 Solution curves showing allowable combinations of frequency and wavelength for bending wave propagation by a flagellar model. The *upper* solid curve is obtained from Eq. 11, with $E_B = 2 \times 10^8$ pN nm^2, $m_o = 20$ pN, $\kappa_o = 0.0002$ rad nm^{-1}, and $k_1/E_{SCB} = 250$ s^{-1}. The *lower* solid curve is obtained by numerical integration of Eqs. 2 and 7, using values of $k_1 = 1{,}000$ s^{-1} and $E_{SCB} = 4$, as in the model shown in Fig. 1. The dashed curve is the same curve plotted with a twofold expansion of the wavelength scale. The solid point gives the values of frequency and wavelength obtained from the computation shown in Fig. 1. The *lower* open point gives the values of frequency and wavelength obtained from the computation shown in Fig. 4.

The boundary condition for 0 shear force at the distal end of the flagellum also requires that there be 0 curvature at the distal end. This boundary condition does not appear to influence the wavelength and frequency of the solution obtained from the flagellar simulations. Simulations similar to Fig. 1 were performed with the flagellar length varied at 2-μm intervals over the range from 32 to 50 μm. Although the bending behavior at the distal end of the flagellum varied, there was no significant variation in the bending behavior of the basal end and mid-region of the flagellum, and the wavelength obtained for the propagated bending waves varied only within the range of 20.9 to 21.4 μm.

The particular solution chosen by the flagellar model does seem to be sensitive to conditions at the basal end of the flagellum. One way to demonstrate this is by changing the control procedure near the basal end so that the switching of m_A in segments 2 to n_1 is controlled by $\kappa(n_1)$.

Fig. 4 shows the result obtained with $n_1 = 4$. This result has values of $L = 29.7$ μm and $f = 27.5$ Hz. A corresponding solution point and a solution point for $n_1 = 3$, giving $L = 26.9$ and $f = 29.8$, are shown in Fig. 3 (open circles).

The boundary condition that must be satisfied at the basal end of the flagellum is $\sigma(0, t) = 0$. Consequently, $\dot{\sigma}(0, t) = 0$. This condition is incompatible with propagation of a uniform wave of curvature (and $\dot{\sigma}$) described by Eq. 9. The analytical solution that was based on Eq. 9 assumed a bend of constant length propagating along the flagellum. Since these bends must be initiated at the basal end of the flagellum, there must be at least one bend at the basal end that is continuously increasing in length and total bend angle. With just one such bend, it is not possible to satisfy both the boundary condition for 0 shear at the base and Eq. 9 for bending wave propagation in distal regions of the flagellum, because the increasing bend angle of the developing bend requires sliding ($\dot{\sigma}$) in the more distal regions of the flagellum, so that $\dot{\sigma}$ is not determined by Eq. 9. However, if there are two developing bends at the basal end that are increasing in angle at equal and opposite rates, the values of $\dot{\sigma}$ in bends distal to these two bends will be independent of events in the developing bends, so that Eq. 23 can be used in the distal part of the flagellum. This situation appears to obtain, at least approximately, in real flagella (Goldstein, 1975; 1976). With this pattern of bend initiation, the bend closest to the basal end grows to approximately half its final bend angle in its first half-cycle of existence and completes its growth during the next half-cycle.

During most of the period of bend development, the solution method used to obtain the curves in Fig. 3 is not applicable to the region of constant m_A closest to the basal end, because the value of curvature at the basal end will be varying. However, there will be one time point at which the magnitude of the curvature at the basal end will be equal to κ_0. This will be the time at which the sign of m_A at the basal end switches, and a new region is initiated. At this time point, and only at this time point, the solution method will also be applicable to the region of constant m_A closest to the basal end. However, the length of this region will be less than that of an active region propagating in the more distal portion of the flagellar model. This is possible because, as shown by the curves in Fig. 3, there are two possible values of wavelength at every frequency at which the model can operate. The operating point can then be established by the relative values of the two wavelengths, as determined by the pattern of bend initiation. In the simplest case, where both the bend angles and the lengths of the bends grow linearly during bend development, the length of this developing bend at the base will be half the length of bends propagating in the more distal portion of the flagellar model. Therefore, it might be expected that the flagellar model would operate at a frequency at which the two possible values of wavelength differ by a factor of two. This operating point is indicated by the intersection of the lower solid curve and the dashed curve in Fig. 3. As indicated in Fig. 3, the flagellar model of Fig. 1 operates at values of frequency and wavelength that are reasonably close to the values predicted by this analysis. It diverges further from this solution when larger length segments are used for the computation, or when bend initiation at the basal end is delayed, as in Fig. 4, to give the results shown by the open circles in Fig. 3.

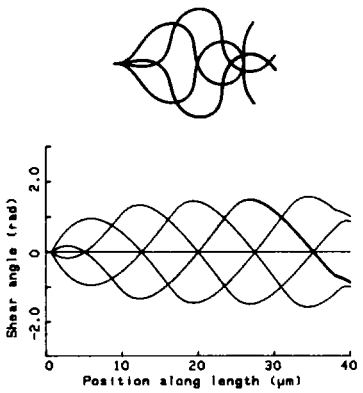

FIGURE 4 Results obtained from computations with a flagellar model identical to the one in Fig. 1, except for a small change in bend initiation at the basal end. The active shear moment generated in segments 2, 3, and 4 of the model is controlled by the curvature at the fourth joint.

Operation in the Presence of External Viscous Resistance

External viscous resistances are introduced by using resistive-force theory (Gray and Hancock, 1955). The drag coefficient values have been increased in the light of more recent hydrodynamic analysis (see Lighthill, 1976; Johnson and Brokaw, 1979). Since the wavelength dependence of the drag coefficients is weak, constant values for these coefficients have been used throughout, with a ratio of C_N/C_L of 1.8.

The bending moments resulting from external viscous resistance of the surrounding fluid depend on the rates of bending of the flagellum via a quadruple integration procedure (Brokaw, 1970, 1972*b*). The integration constants required by this procedure are obtained from boundary conditions for the external forces and moments applied to the ends of the flagellum. Only the case where both ends of the flagellum are free, so that no external forces or moments are applied at the ends, is considered here. Details of the external viscous resistance terms that need to be used have been given in previous work (Brokaw, 1972*b*). Since these terms depend on the values of $\kappa(s, t)$ at the beginning of a time interval, the external viscous resistances are handled in an explicit rather than an implicit manner. Since these are viscous terms, this results in inaccuracy rather than instability of the solution process. An alternative approach that avoids these inaccuracies is described by Hines and Blum (1978).

Figs. 2 *b* and 5 show the results of computing the movement of this flagellar model at a relative viscosity of 8, i.e., an external viscosity eight times higher than the value normally used for observations of sea urchin sperm flagella, by using a value of 0.0173 N s m^{-2} for the tangential drag coefficient, C_L. The internal elastic bending resistance, E_B, was varied, as in Fig. 2 *a*, over the range from 0.8×10^8 to 2.9×10^8 pN nm^2, with a constant value of m_o. At increased external viscosities the movement of the model was found to be more stable if a small amount of internal elastic shear resistance, E_S, was included. E_S was given a value of 2.0 pN when $E_B = 1.0 \times 10^8$ pN nm^2, and was varied proportionately as E_B was varied. In contrast to the smooth change in wavelength obtained in the absence of external viscosity (Fig. 2 *a*), three stable wavelength modes were found (Fig. 2 *b*). Within each of these modes, the wavelength was nearly independent of the elastic resistances. Intermediate values of wavelength between these modes were not stable.

The wavelength mode that is stable from $E_B = 1.1 \times 10^8$ pN nm^2 to 2.6×10^8 pN nm^2 is illustrated in Fig. 5 *b*. This mode has approximately two complete bending waves on the flagellum. The frequency of oscillation decreases gradually from 13.8 Hz at $E_B = 1.1 \times 10^8$ pN nm^2 to 9.7 Hz at 2.6×10^8 pN nm^2.

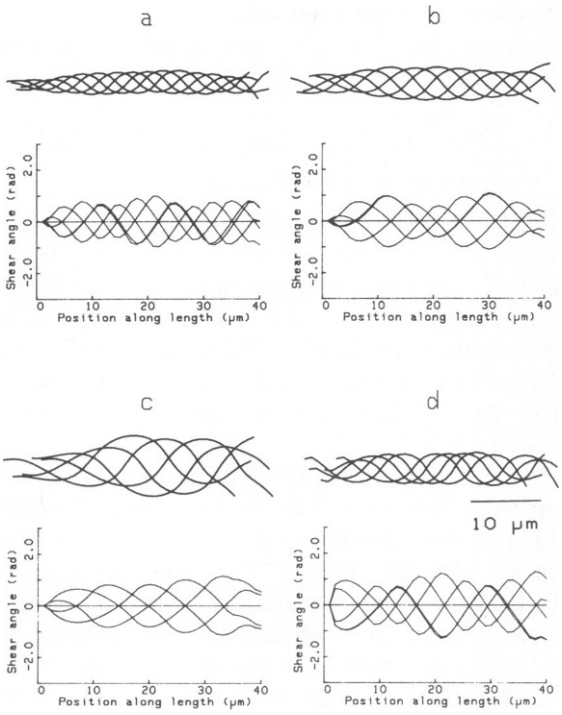

FIGURE 5 Waveforms obtained at the three stable wavelength modes identified by the computations summarized in Fig. 2 *b*. Each panel shows one cycle of the motion plotted at ¼ cycle intervals, with the motion in the *x*, *y* plane shown above a plot of shear angle as a function of length. (*a*) With $E_b = 1.1 \times 10^8$ pN nm^2 and $E_S = 2.2$ pN; the frequency is 22.3 Hz. (*b*) With $E_B = 1.9 \times 10^8$ pN nm^2 and $E_S = 3.8$ pN; the frequency is 12.7 Hz. (*c*) With $E_B = 2.8 \times 10^8$ pN nm^2 and $E_S = 5.6$ pN; the frequency is 5.1 Hz. (*d*) Waveform obtained by driving the oscillation at a frequency of 16.5 Hz, to obtain a wavelength in between the wavelengths produced in *a* and *b*. $E_B = 1.2 \times 10^8$ pN nm^2 and $E_S = 3$ pN. Computations were performed with the flagellar length divided into 40 segments and with 80 time steps per cycle of oscillation.

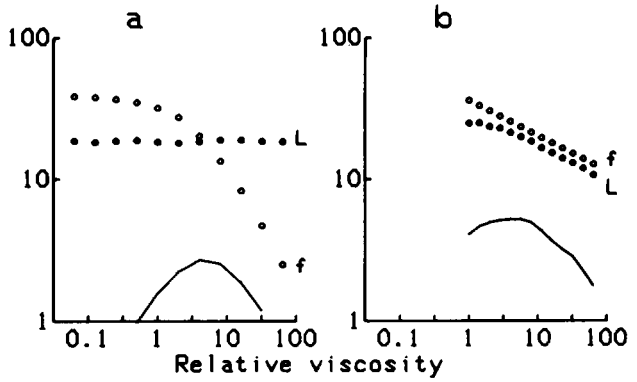

FIGURE 6 Effect of viscosity on parameters of the flagellar model. Wavelengths are indicated by the solid points, frequencies are indicated by the open points, and the power (averaged over one cycle), in units of 10^{-2} pJ/s, is indicated by the solid line. (*a*) Free oscillations of the same model shown in Fig. 5 *b*, with $E_B = 1.2 \times 10^8$ pN nm^2 and $E_S = 3$ pN. (*b*) Forced oscillations of a slightly modified model, with $E_B = 2.0 \times 10^8$ pN nm^2, $E_S = 4.8$ pN, $m_o = 32$ pN, and $\kappa_1 = 1{,}500\ s^{-1}$. The frequencies were chosen so that log (frequency) $-\frac{1}{4}$ log (viscosity) is constant.

In the lower portion of this range of elastic resistances, up to $E_B = 1.6 \times 10^8$ pN nm^2, a mode with approximately three complete bending waves is stable (Fig. 5 *a*). This mode has a higher frequency of oscillation, decreasing from 23.2 Hz at 0.8×10^8 pN nm^2 to 20.4 Hz at 1.6×10^8 pN nm^2. In the region in which two stable modes are shown, the mode obtained depends upon the initial conditions.

At the upper end of this range of elastic resistances, beginning at $E_B = 2.65 \times 10^8$ pN nm^2, there is one stable mode with a wavelength of ~26.4 μm and frequencies of ~5 Hz (Fig. 5 *c*).

At $E_B = 1.2 \times 10^8$ pN nm^2 the wavelength obtained in the absence of external viscosity is similar to the wavelength of the two-wave mode obtained at high viscosity, and the relative external viscosity can be varied from 0 to 64, with no significant change in the wavelength (Fig. 6 *a*). The average power expended against the external viscous resistance is also plotted in Fig. 6. The maximum power output is obtained at a viscosity where the frequency of oscillation has been reduced to half the frequency obtained in the absence of external viscosity; the active shear system in this model has a maximum power output at half the maximum shear rate.

Fig. 7 compares the characteristics of the solutions obtained at relative viscosities of 0, 1, 8, and 64. The third row of Fig. 7 shows the relationship between curvature and active shear moment along the length of the flagellar model at single time points in the oscillation cycle. The curvature curves indicate that bends propagate along the flagellum with approximately the same wavelength

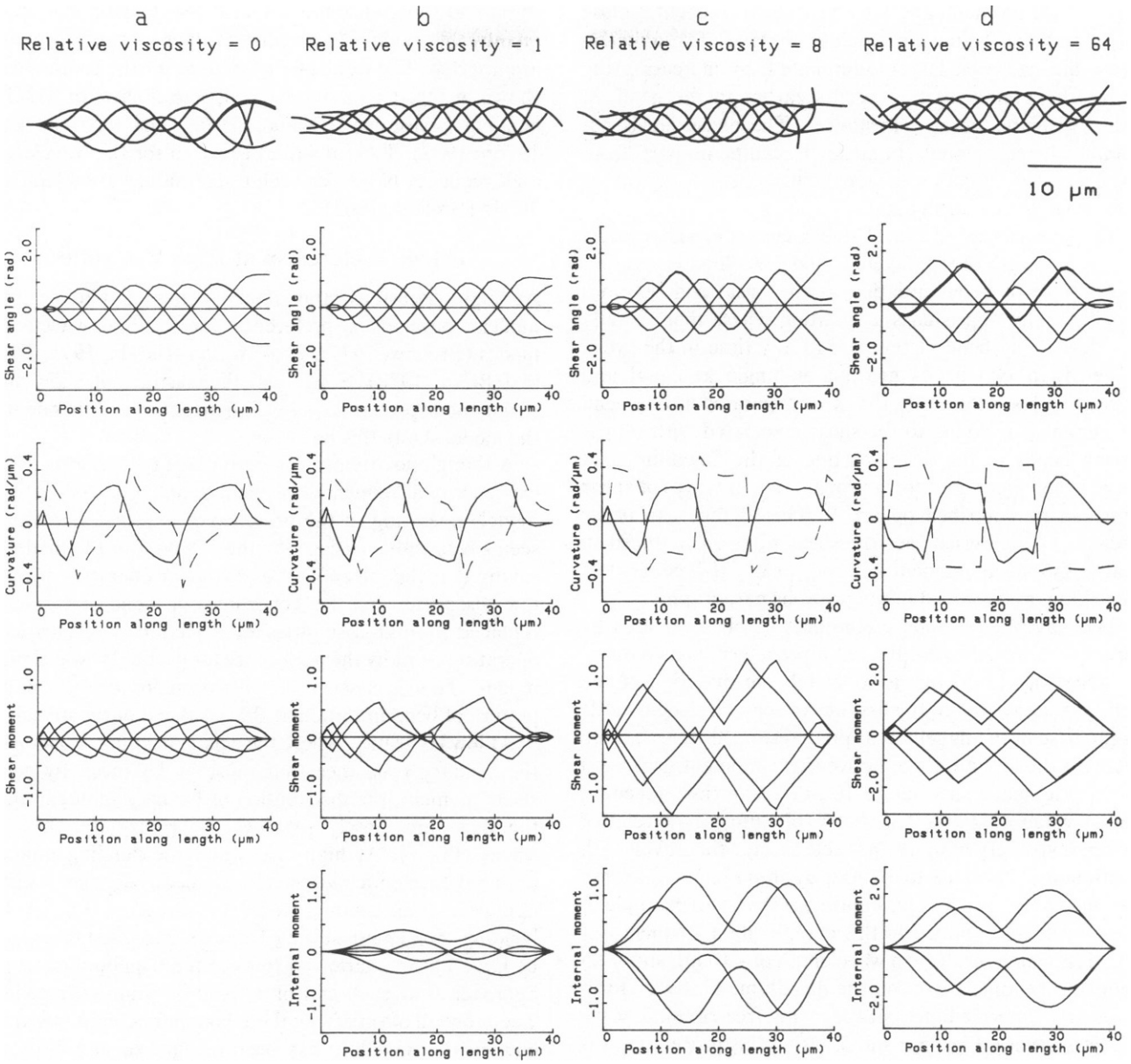

FIGURE 7 Waveforms obtained from computation of free oscillation of the flagellar model used to obtain the data in Fig. 6 *a*, shown at relative viscosities of 0, 1, 8, and 64. At each viscosity, the motion in the *x*, *y* plane is shown at the *top* of the column. The plot labeled curvature shows only one curve of curvature vs. length, given by the solid curve, for comparison with a curve at the same time in the cycle for active shear moment per unit length, *m*, given by the dashed line. The units for *m* are 50 pN. The plot labeled shear moment gives the bending moments resulting from integration of the active shear forces and the forces generated by elastic shear resistance. The plot labeled internal moment gives the sum of the bending moments resulting from shear forces and the bending moment resulting from the elastic bending resistance. This sum must, therefore, be equal in magnitude to the moment resulting from external viscous resistances. The units for both plots of bending moments are 10^5 pN nm; but note that the scale is compressed by a factor of two for the plots at a relative viscosity of 64.

throughout this range of viscosities, although there is some change in the shape of the bends. On the other hand, increasing the viscosity causes a dramatic change in the shape of the curves showing active shear moment along the length. At low viscosities, the frequency and sliding velocity are high. In the regions of the bending wave where sliding is occurring at a near-maximal velocity, the active shear moment is greatly reduced. Near the trailing edge of a bend, as the sliding velocity falls, the active shear moment increases towards its maximal value. As a result, there is a sharp peak in the trailing portion of the shear moment curves. This is equivalent to a phase lag between the curvature curve and the shear moment curve, which provides part of the phase lag that is needed to achieve equilibrium between the active shear moment and the elastic resistances (Brokaw, 1971). At high viscosities, on the other hand, the frequency and the sliding velocities are reduced, so that there is little effect of sliding velocity on

active shear moment, and the active shear moment is close to its maximal value throughout the bend. The effective phase lag has been largely eliminated, by increasing the active shear moment that occurs earlier in the bend, in phase with the viscous resistances. The phase lag is not completely eliminated, because it results in part from switching the direction of active shear at $+/-\kappa_0$ rather than when the curvature is 0.

The second row of Fig. 7 shows curves of shear angle along the length of the flagellar model. At high viscosities, the pattern of bend initiation at the basal end becomes modified, and approaches a situation where there is only one developing bend at the base at any time in the cycle, rather than two bends growing in angle at equal and opposite rates. As a result, the shear generated during bend development is added to the shear associated with propagating bends in the distal portion of the flagellum, and there is no longer a uniform propagation of waves of shear that can be described by Eq. 9. This change can occur because at high viscosities the shear rates are reduced so that active shear moment becomes nearly independent of shear rate, as discussed in the previous paragraph.

The wavelength mode preferences can be overriden by forcing the model to oscillate at a predetermined frequency. One way to do this is to switch the direction of the active shear system in the first active segment (segment 2) at the base of the flagellum at predetermined times, and to increase the magnitude of active shear moment generated in this segment to a value of 10 m_0. Using this procedure and a value of $E_B = 1.2 \times 10^8$ pN nm^2, at a relative external viscosity of 8, it is possible to vary the wavelength continuously from 18 to 10 μm, by imposing frequencies varying from 13 to 34 Hz. Figure 5 *d* shows an example of the movement obtained in this case, using a frequency of 16.5 Hz, which results in a wavelength of ~16 μm and ~2.5 complete bending waves on the flagellum. This waveform is clearly intermediate between the free-running wave modes shown in Figs. 5 *a* and *b*. Using this procedure, it is also possible to obtain a continuous decrease in wavelength as the viscosity is increased by specifying either a constant frequency or a frequency that decreases in a realistic manner with increasing viscosity (Fig. 6 *b*).

DISCUSSION

Operation at 0 Viscosity

Flagella normally operate in an environment where viscous resistances of the fluid are significant. A model operating at 0 viscosity may be relevant to situations where flagella generate normal-looking bending waves at very low beat frequencies (Brokaw, 1966; 1975*a*).

The model examined here demonstrates that bend propagation by curvature-controlled flagellar models is not dependent upon interaction with the viscous resistance of the surrounding fluid environment. Bending wavelengths similar to those encountered with real flagella are generated by this model when realistic values for the parameters are inserted. The value of E_B/m_0 used for the computation shown in Fig. 1 is based on realistic estimates of flagellar bending resistance (Okuno, 1980) and m_A (Brokaw, 1975*b*; 1982). Typical values reported for the wavelength and frequency of live sea urchin spermatoza are 30 μm and 30 Hz (Brokaw, 1965).

Mode Preferences at High Viscosities

At high viscosities, this flagellar model, like previous models, develops a preference for discrete wavelength modes (Brokaw, 1972*c*; Brokaw and Rintala, 1975; Hines and Blum, 1978). Since real flagella do not show such strong mode preferences, it is important to understand why the model shows this behavior.

Although no attempt has been made to demonstrate the existence of a frequency-wavelength map such as Fig. 3 for models operating in the presence of external viscosity, it seems reasonable to describe the behavior of the model by saying that the selection of a particular operating point at low viscosities by the conditions of bend initiation is replaced at high viscosities by selection of a particular operating point by the preference for particular wavelength modes. This is associated with a major change in the pattern of bend initiation at the basal end of the model.

At low viscosities, where the elastic bending resistance is the primary resistance that must be balanced by active shear moment, the distribution of bending moment along the flagellum closely matches the propagated bending waves (Fig. 7). At high viscosities, the bending moment required to balance viscous resistances becomes a dominant part of this bending moment distribution (Fig. 7). The bending moments resulting from viscous resistances must be large in the interior portions of the flagellum and must approach 0 at each end of a freely swimming flagellum. The problem of satisfying these boundary conditions at the ends of the flagellum has been recognized and discussed previously (Brokaw, 1970, 1971). It was previously suggested that nonuniformities in bend propagation would be required in a curvature-controlled flagellum to satisfy these boundary conditions. The flagellar models actually solve this problem differently. They take advantage of the degree of freedom represented by the frequency-wavelength map of Fig. 3 to select operating wavelengths giving integral numbers of bends on the flagellum, so that the active bending moment, obtained by integrating the active shear moment along the length of the flagellum, will be 0 at the base of the flagellum. At high viscosities, where the active shear moment is independent of shear rate and is therefore determined entirely by the curvature-control specification, a uniform, symmetrical bending wave will generate equal amounts of active shear moment in each direction, and the integrated active bending moment over one full wave will be 0 (Fig. 7).

Viscosity-Independence of the Wavelength

In the series of computations summarized by Figs. 6 *a* and 7, the beat frequency decreases enough so that there is no change in wavelength over a wide range of viscosities. This behavior contrasts with the behavior of real flagella and with the behavior of the curvature-controlled models examined earlier (Brokaw, 1972*c*; Hines and Blum, 1978). With the previous models, the wavelength changed to progressively lower modes, with a greater number of complete waves on the flagellum, as the viscosity was increased. The difference between the behavior of the model discussed here and the previous models is probably due to the time delay that was explicitly included in the control loop of the previous models. Hines and Blum (1978) pointed out that the equations that they used for solving the balance of moments could be expressed in dimensionless form in which the viscosity appeared only as the ratio of drag coefficients, C_N/C_L, or as a ratio between C_N and the time constant that they used to delay the active shear moment. Computations with curvature-controlled models containing an explicit time delay show that there is no change in wavelength with viscosity if the ratio between the time delay and the viscosity is kept constant (data not shown). These considerations suggest that if the mechanism of oscillation in real flagella is anything like the curvature-controlled models that have been examined, then the mechanism in real flagella must contain a time delay that remains approximately constant as the viscosity is increased.

Conclusion

The fundamental idea of this analysis is that flagellar bending represents the solution of a moment balance equation containing active bending moment resulting from a specification of the activity of an active shear process by feedback from a parameter such as the curvature of the flagellum. Concern about the strong wavelength mode preferences exhibited by flagellar models of the type examined here has led to previous suggestions that this approach might be inapplicable to real flagella (Brokaw, 1980). The most important new understanding presented here is that controlling the active shear process by curvature does not fully determine the operating parameters of this type of flagellar model, but only determines a curve of possible combinations of frequency and wavelength that will satisfy the moment balance equation. Some other conditions, such as the details of bend initiation at the basal end of the flagellum when the model is operating at low viscosity or the preference for wavelength modes that facilitate satisfaction of the boundary condition for 0 active moment at the basal end when the model is operating at high viscosity, will determine the solution that is chosen. It is also possible to override these conditions by driving the flagellar model at a particular frequency, in which case the wavelength will be determined by the moment balance equation and will decrease smoothly with increasing viscosity (Rikmenspoel, 1982). The observation that real flagella do not show the pronounced wavelength mode preferences that are seen with these models therefore does not eliminate these models as candidates for the mechanisms in real flagella, but does suggest that other properties are required to explain how real flagella select a particular operating point. The idea that real flagella contain a mechanism that predetermines a particular frequency, such as the model that produced the results in Fig. 5 *d* and 6 *b* or the more complicated model examined by Rikmenspoel (1982) is difficult to reconcile with the effect of viscosity on reducing the oscillation frequency of flagella (e.g., Brokaw, 1966; Rikmenspoel, 1984). The manner in which real flagella resolve this problem remains to be determined.

I am happy to thank Drs. J. J. Blum and M. Hines for valuable comments on earlier versions of this manuscript.

This work has been supported by grants from the National Institutes of Health, GM 18711 and GM 21931.

Received for publication 2 January 1985 and in final form 31 May 1985.

REFERENCES

Brokaw, C. J. 1965. Non-sinusoidal bending waves of sperm flagella. *J. Exp. Biol.* 43:155–169.

Brokaw, C. J. 1966. Effects of increased viscosity on the movements of some invertebrate spermatozoa. *J. Exp. Biol.* 45:113–139.

Brokaw, C. J. 1970. Bending moments in free-swimming flagella. *J. Exp. Biol.* 53:445–464.

Brokaw, C. J. 1971. Bend propagation by a sliding filament model for flagella. *J. Exp. Biol.* 55:289–304.

Brokaw, C. J. 1972*a*. Flagellar movement: a sliding filament model. *Science (Wash. DC).* 178:455–462.

Brokaw, C. J. 1972*b*. Computer simulation of flagellar movement. I. Demonstration of stable bend propagation and bend initiation by the sliding filament model. *Biophys. J.* 12:564–586.

Brokaw, C. J. 1972*c*. Computer simulation of flagellar movement II. Influence of external viscosity on movement of the sliding filament model. *J. Mechanochem. Cell Motil.* 1:203–211.

Brokaw, C. J. 1975*a*. Effects of viscosity and ATP concentration on the movement of reactivated sea urchin sperm flagella. *J. Exp. Biol.* 62:701–719.

Brokaw, C. J. 1975*b*. Cross-bridge behavior in a sliding filament model for flagella. *In* Molecules and Cell Movement. S. Inoue and R. E. Stephens, editor. Raven Press, New York. 165–179.

Brokaw, C. J. 1980. Theoretical models for oscillation and bend propagation by sperm flagella. *In* Testicular Development, Structure and Function. A. Steinberger and E. Steinberger, editors. Raven Press, New York. 447–453.

Brokaw, C. J. 1982. Models for oscillation and bend propagation by flagella. *Symp. Soc. Exp. Biol.* 35:313–338.

Brokaw, C. J., and D. R. Rintala. 1975. Computer simulation of flagellar movement. III. Models incorporating cross-bridge kinetics. *J. Mechanochem. Cell Motil.* 3:77–86.

Goldstein, S. F. 1975. Morphology of developing bends in sperm flagella. *In* Swimming and Flying in Nature, T. Y.-T. Wu, C. J. Brokaw, and C. Brennen, editors, Plenum Publishing Corp., New York. 127–132.

Goldstein, S. F. 1976. Form of developing bends in reactivated sperm flagella. *J. Exp. Biol.* 64:173–184.

Gray, J., and G. J. Hancock. 1955. The propulsion of sea urchin spermatozoa. *J. Exp. Biol.* 32:802–814.

Hines, M., and J. J. Blum. 1978. Bend propagation in flagella. I. Derivation of equations of motion and their simulation. *Biophys. J.* 23:41–57.

Hines, M., and J. J. Blum. 1979. Bend propagation in flagella. II. Incorporation of dynein cross-bridge kinetics into the equations of motion. *Biophys. J.* 25:421–442.

Johnson, R. E., and C. J. Brokaw. 1979. Flagellar hydrodynamics. A comparison between resistive-force theory and slender-body theory. *Biophys. J.* 25:113–127.

Kinoshita, H., and T. Kamada. 1939. Movement of abfrontal cilia of *Mytilus*. *Jpn. J. Zool.* 8:291–310.

Lighthill, J. 1976. Flagellar hydrodynamics. *Soc. Ind. Appl. Math. Rev.* 18:161–230.

Machin, K. E. 1958. Wave propagation along flagella. *J. Exp. Biol.* 35:796–806.

Machin, K. E. 1963. The control and synchronization of flagellar movement. *Proc. R. Soc. Lond. B. Biol. Sci.* 158:88–104.

Okuno, M. 1980. Inhibition and relaxation of sea urchin sperm flagella by vanadate. *J. Cell Biol.* 85:712–725.

Rikmenspoel, R. 1982. Ciliary contractile model applied to sperm flagellar motion. *J. Theor. Biol.* 96:617–645.

Rikmenspoel, R. 1984. Movements and active moments of bull sperm flagella as a function of temperature and viscosity. *J. Exp. Biol.* 108:205–230.

Shingyoji, C., A. Murakami, and K. Takahashi. 1977. Local activation of triton-extracted flagella by iontophoretic application of ATP. *Nature (Lond.).* 265:269–270.